Author/s:
Duthie, X;Kentish, S;Powell, C;Nagai, K;Qiao, G;Stevens, G

Title:
Operating temperature effects on the plasticization of polyimide gas separation membranes

Date:
2007-05-15

Citation:
Duthie, X., Kentish, S., Powell, C., Nagai, K., Qiao, G. & Stevens, G. (2007). Operating temperature effects on the plasticization of polyimide gas separation membranes. Journal of Membrane Science, 294 (1-2), pp.40-49. https://doi.org/10.1016/j.memsci.2007.02.004.

Persistent Link:
https://hdl.handle.net/11343/55670

Operating Temperature Effects on the Plasticization of Polyimide Gas Separation Membranes

Xavier Duthie[1], *Sandra Kentish*[1*], *Clem Powell*[1], *Kazukiyo Nagai*[1,2], *Greg Qiao*[1], *Geoff Stevens*[1]

[1]Cooperative Research Centre for Greenhouse Gas Technologies (CO2CRC), Department of Chemical and Biomolecular Engineering, The University of Melbourne, 3010, Victoria, Australia.

[2]Department of Applied Chemistry, Meiji University, Kawasaki, 214-8571, Japan

*Corresponding author: sandraek@unimelb.edu.au

Abstract

Membrane plasticization is the process whereby penetrant dissolution causes membrane swelling or dilation, which in turn, can increase membrane diffusivity and solubility and lead to long time frame polymer relaxation processes. In this work, the effect of temperature upon the plasticization of a rigid polyimide, poly(4,4'-hexafluoroisopropylidene diphthalic anhydride - 2,3,5,6-tetramethyl-1,4-phenylenediamine) (6FDA-TMPDA), by carbon dioxide is investigated. It is found that across the full range of temperatures studied, plasticization has little effect on carbon dioxide solubility as all results can be characterized by a standard dual mode sorption model. However, the effect upon diffusivity is significant and this can be described by both an exponential relationship with penetrant concentration and an Arrhenius relationship with temperature. The polymer relaxation processes induced by plasticization are also temperature dependent. However, the total proportion of penetrant sorption associated with such relaxation processes is relatively unaffected by temperature. This paper shows that plasticization effects are dominated by Henry's law dissolution. Conversely, while Henry's Law species contribute most to diffusion at high temperatures, at lower temperatures the movement of Langmuir component species also contributes to the total diffusion coefficient.

Keywords: plasticization; polyimide; permeability; solubility; diffusivity

Introduction

The use of polyimide membranes for the separation of carbon dioxide from other gases is of increasing commercial interest. Of particular concern in this field is the prevention, or at least suppression, of plasticization. This phenomenon is induced by medium to high concentrations of hydrocarbons and polarizable gases, including carbon dioxide. Conceptually, plasticization can be thought of as a swelling and slight solvation of the polymer by the plasticizing gas. This affords greater mobility to the polymer chains, often interpreted as more void space. Current conceptual models of the plasticization / swelling phenomenon suggest that it is primarily due to dissolution of gas into micro-voids that are smaller than the gas molecule diameter, that is, Henry region dissolution [1]. This 'molecular misfit' implies that the polymer matrix must swell to accommodate the gas, leading to permanent damage to the matrix. This, in turn leads to larger inter-chain spacing in the polymer, and dramatic increases to gas and vapour diffusion coefficients.

The focus of the present paper is the common glassy polyimide poly(4,4'-hexafluoroisopropylidene diphthalic anhydride - 2,3,5,6-tetramethyl-1,4-phenylenediamine) (6FDA-TMPDA). This rigid fluorinated polyimide has previously been the subject of a number of CO_2-based gas separation studies [2-7]. It shows very high permeabilities, while retaining reasonable selectivities. Some work has been done to characterize its thermal properties; including variation of gas permeability and selectivity. Similarly, several works have examined the plasticization phenomenon in polyimide gas separation membranes, with Bos *et al.* [8-12] examining primarily BTDA-based polyimides over a narrow temperature range, Okamoto *et al.* [13] using BPDA systems and both Wind *et al.* [14, 15] and Wessling *et al.* [16] focusing on polyimides synthesized from the dianhydride 6FDA. However, the thermal dependence of plasticization in such systems is not well described. It is the purpose of the present paper to study the plasticization performance of the polyimide 6FDA-TMPDA during exposure to carbon dioxide across an extended temperature range.

Theory

Membrane permeability (P) is the well known product of the thermodynamic diffusion coefficient (D_T) and the solubility (S). The thermodynamic diffusion coefficient is in turn related to the Fickian diffusion coefficient (D) by [17]:

$$D = D_T S \frac{df}{dC} \qquad \textbf{Equation 1}$$

where f is the fugacity of the penetrant in the gas phase and C is its concentration within the polymer.

The temperature dependence of the permeability, solubility and diffusivity of a penetrant in a polymeric membrane may be described by two Arrhenius expressions and a van't Hoff relationship [18]:

$$P = P_o e^{-E_P/RT} \quad \textbf{Equation 2}$$

$$D = D_o e^{-E_D/RT} \quad \textbf{Equation 3}$$

$$S = S_o e^{-H_S/RT} \quad \textbf{Equation 4}$$

where P_o, D_o and S_o are pre-exponential factors, E_p is the activation energy for permeation, E_D is the activation energy for diffusion and H_S is the heat of sorption.

For glassy polymers, the concentration dependence of the solubility is often characterized by a dual mode sorption model [17, 19]. This model regards the glassy polymer as having two domains into which penetrant gas can sorb. The first is the standard model of Henry's law dissolution; gas literally dissolves into free volume between adjacent polymer chains. Due to the variation in a polymer's molecular structure, fluctuations in chain molecular diameter occur, providing opportunity for gas to dissolve. Conversely, in the Langmuir domain gas is adsorbed into the excess free volume. Excess free volume may be thought of as microscopic voids in a polymer sample. These voids are created when polymer chains pack imperfectly, and are present in the glassy state, but importantly, not the rubbery state. The total concentration of sorbed penetrant (C) is thus composed of a dissolved component (C_D) and adsorbed component (C_H):

$$C = C_D + C_H = K_D f + \frac{C_H^{'}.b.f}{1+bf} \quad \textbf{Equation 5}$$

where K_D is the Henry's Law coefficient, $C_H^{'}$ is the Langmuir capacity constant and b is the Langmuir affinity constant. The gas phase penetrant concentration is presented as a fugacity, f, rather than a pressure, to more correctly represent the chemical potential of the species in the gas phase.

Inherent to Equation 5 is the assumption that the sorption parameters are not dependent on penetrant fugacity. However, concentration dependence is commonplace in analysis of Henry's law sorption for amorphous rubbery polymers [20]. Similarly, it has also been shown that increasing concentrations of a plasticizing penetrant can cause the glass transition temperature to decrease. This would imply that the Langmuir sorption capacity is also concentration dependent [1,21-22]. The extended dual mode sorption model accounts for such effects [21]:

$$C = K_D \exp(\sigma C^*) f + \frac{C_H^{'}(0) bf (1 - C^*/C_g)}{1+bf} \quad \textbf{Equation 6}$$

$C_H^{'}(0)$ is the value of the Langmuir capacity extrapolated to a penetrant concentration of zero, C^* is the effective concentration of penetrant in the polymer and C_g is the penetrant concentration required to induce glass transition in a polymer at a given operating temperature. σ is a parameter characterizing the concentration dependence of the Henry's Law dissolution [1].

For unplasticized glassy polymers, the dual mode sorption model allows the permeability to be modeled by [23]:

$$P = K_D D_{TD} + C_H^{'} D_{TH} \frac{\ln(1+bf)}{f} \quad \textbf{Equation 7}$$

In this case, the penetrant diffusivity is interpreted as having two contributions; one describing the diffusion of penetrant dissolved in the Henry region, D_{TD}, and another describing the diffusion of penetrant adsorbed in Langmuir 'holes', D_{TH}.

For plasticizing polymers, this relationship has been shown to be inadequate since it implies that the respective diffusions constants are not concentration dependent. As discussed by Platé and Yampol'skii [24], the dependence of the diffusion coefficient on free volume is well established [25].

$$D = A\exp\left(-B/\upsilon_f\right) \quad \textbf{Equation 8}$$

Where A and B are constants related to penetrant sterics, and υ_f is the fractional free volume. As the polymer swells under plasticization, this relationship in turn leads to a diffusion coefficient that is also a function of penetrant concentration. A number of workers [26, 27], have shown that this concentration dependence can be expressed through:

$$D = D(0)\exp(\beta C) \quad \textbf{Equation 9}$$

where β accounts for the plasticizing ability of the penentrant and D(0) is the diffusion coefficient in the limit of zero penetrant concentration.

For permeation across a planar nonporous membrane of thickness δ, from an upstream gas fugacity f_1 to downstream f_2 the effective permeability coefficient is given by:

$$\overline{P} = \frac{J_s\delta}{(f_1 - f_2)} \quad \textbf{Equation 10}$$

where J_s is the steady state flux across the membrane:

$$J_s = D\frac{\delta C}{\delta x} \quad \textbf{Equation 11}$$

Manipulation of Equations 5, 9, 10 and 11, assuming f_2=0 yields:

$$\overline{P} = \frac{D(0)}{\beta f_1}\left(\exp\left(\beta K_D f_1 + \frac{\beta C'_H\, b.f_1}{1+bf_1}\right) - 1\right) \quad \textbf{Equation 12}$$

Paul and Koros [28] argue that the penetrant in Langmuir voids is less mobile than that fully dissolved in the Henry's law regime. They introduced a parameter, F to represent the fraction of the Langmuir species that are fully mobile, while (1-F) species remain totally immobilized. Stern *et al.* [29] extended Equations 9 and 12 to include this parameter:

$$D_{eff} = D(0)\exp\left[\beta K_D f\left(1+\frac{F.K}{1+bf}\right)\right].\left[\frac{1+\frac{F.K}{(1+bf)^2}}{1+\frac{K}{(1+bf)^2}}\right] \qquad \textbf{Equation 13}$$

$$\overline{P} = \frac{D(0)}{\beta f_1}\left(\exp\left(\beta K_D f_1\left(1+\frac{F.K}{1+bf_1}\right)\right)-1\right) \qquad \textbf{Equation 14}$$

where $K = C_H'.b/K_D$. Okamoto *et al.* [13] found that for CO_2 transport in BPDA-based polyimide, the model of Stern *et al.*[29] gave a much better fit for permeability data.

Finally, a number of workers have shown that the stretching of polymer void space that occurs with plasticization takes place over quite long time frames and it is these polymer relaxation processes that lead to the time dependence of permeation in plasticizing membranes. The sorption process is described as having two components, a relatively fast Fickian dissolution of penetrant (ϕ_F), followed by a much slower relaxation step (ϕ_R). Thus the sorbed mass uptake, M(t), can be expressed as[14, 16, 29]:

$$\frac{M(t)-M_0}{M_\infty - M_0} = \phi_F(t) + \phi_R(t) \qquad \textbf{Equation 15}$$

If the polymer relaxation process is assumed to follow first order kinetics, this contribution may be described by:

$$\phi_R(t) = \phi_R\left[1-\exp\left(-\frac{t}{\tau_R}\right)\right] \qquad \textbf{Equation 16}$$

where the rate of relaxation is characterized by a relaxation time τ_R. This relaxation time can be converted to a relaxation rate constant by [16]:

$$K_R = \frac{\delta^2}{\tau_R} \qquad \textbf{Equation 17}$$

where δ is the membrane thickness.

Wessling *et al.* [16] show that at low pressures, the bulk of penetrant sorption occurs in a classical Fickian manner, whereas at higher penetrant pressures, larger proportions of the total penetrant dissolution occur through polymer relaxation.

Experimental

The fluorinated polyimide poly(4,4'-(Hexafluoroisopropylidene)diphthalic anhydride - 2,3,5,6-tetramethyl-1,4-phenylenediamine), (6FDA-TMPDA) was the polymer of interest in this study, with the structure given in Figure 1.

The polymer was synthesized via a method described previously [31, 32] and dissolved in dichloromethane (AR grade, used as received from Ajax Finechem) at a concentration of 2.5 $^{wt}/_{vol}$%. Solutions were filtered through 0.75 µm glass fibre filters (Advantec), before being solution cast using glass casting rings. Drying was complete in two stages [33]. Initial drying was at room temperature for approximately 48 hrs, with the casting ring covered with a Petri dish, ensuring a near-saturated environment immediately above the membrane. Films were then removed from glassware using distilled water, before being dried *in-vacuo* firstly at 80°C for 15 hrs, then at 150°C for 48 hrs. Absolute pressure in the vacuum oven was approximately 3 kPa. Membranes were stored in a desiccator until use. Membrane thicknesses were measured using a micrometer (Mitutoyo, Japan) with an accuracy of approximately ± 1 µm. The measured thickness varied between 40 and 50 µm.

The solubility of CO_2 in the polyimide films under consideration was measured using a Cahn 2000 microbalance, coupled with a chart recorder. The microbalance was housed in a temperature controlled, purgable, stainless steel pressure vessel. The measurement was conducted by admitting gas at the required pressure into the system, and monitoring the change in mass of the film $(M(t) - M_0)$ until negligible mass increase was observed. This approach to equilibrium took between 6 and 102 hours depending upon the gas temperature and pressure.

The gas pressure was then increased to the next level, and the process repeated. The pressure range was 0 – 40.5 kPa. Experiments were repeated at 21, 35, 50 and 77°C.

Permeabilities were measured with a constant volume, variable pressure gas permeation apparatus (see Figure 2). The apparatus operates by supplying feed gas at a constant pressure to a pre-heating loop before proceeding to a sealed membrane unit. The unit is a dead end Millipore high - pressure filter holder (# XX45 047 00). The heating loop and membrane unit are housed in an oven that is temperature controllable to 300 °C. The permeate gas passes into a cooling loop that is housed in a water bath, ensuring a constant measurement temperature of 27.5 ± 0.2 °C. Data is logged electronically at a rate of 1 read per second, with each data point being an average of 100 individual pressure measurements. CO_2 feed pressures were determined with an MKS Baratron® transducer of range 0 to 7000 kPa absolute pressure, while downstream volumes were measured with an equivalent model of 0 to 1.3 kPa absolute pressure. Feed gas pressures ranged from 330 to 3000 kPa, while operating temperatures ranged from 3 to 112 °C. Measurement of the CO_2 permeability isotherm for the glassy polymer membranes under study followed the protocol outlined in Table 1. This was independent of temperature.

Overnight evacuation of the permeability system was completed at 35 °C, with the system operating temperature adjusted to the required value approximately two hours prior to the nitrogen permeability measurement. Evacuation at a consistent temperature ensured that any annealing that may occur in the membrane due to elevated temperature was minimized. CO_2 fugacities were calculated from experimental pressures and temperatures using the Peng-Robinson equation of state [34]. Estimates of experimental uncertainty were made by replicate measurements, with error bars defined as +/- twice the standard error of the measurement.

The glass transition temperature of 6FDA-TMPDA was measured via Differential Scanning Calorimetry using a Perkin Elmer Diamond DSC. Using a sample size of approximately 5 mg, films were heated at 20 °Cmin^{-1} from 50 °C to 500 °C.

Results and Discussion

Solubility

In order to study the thermal dependence of 6FDA-TMPDA plasticization by carbon dioxide, it is necessary to first understand how the solubility of this penetrant in 6FDA-TMPDA varies with temperature. Using the apparatus detailed earlier, solubility was determined gravimetrically, with carbon dioxide uptake by 6FDA-TMPDA measured as a function of penetrant fugacity across a range of pressures and temperatures.

True to most glassy polymers, 6FDA-TMPDA was measured to have a decreasing solubility with increasing temperature (Figure 3). The data was fitted well by the dual mode sorption model, Equation 5. There is no evidence of an upward inflection point in the high-fugacity region of the graph, indicating that an extended model (Equation 6) is not required. This is not unexpected, as the operating temperature range is a long way below the glass transition temperature of 422 °C (DSC thermogram not shown). Estimates of the dual mode sorption parameters are presented in Table 2. When expressed on a pressure basis, the Henry's Law constant, is comparable to the data of Shao *et al.* [35]. The Langmuir capacity (C_H') is somewhat higher than in this work and the affinity constant (*b*) somewhat lower. This variation in Langmuir parameters probably arises from the differences in drying protocols utilized in membrane preparation.

These sorption parameters can readily be fitted to individual van't Hoff and Arrhenius relationships comparable to Equations 3 and 4 (see Table 3). It can be seen that all three exponent energies are negative, indicating reductions in magnitude with increasing operating temperature, which is in agreement with prior work using BPDA-based polyimides [13].

It is also useful to examine the dynamics of carbon dioxide sorption. For this purpose, it is common to plot the fractional sorbed mass uptake $(M(t) - M_0)/(M_\infty - M_0)$ as a function of the square root of time ($t^{1/2}$) . A system exhibiting true Fickian behaviour should be linear until a fractional mass uptake of at least 0.5 on this basis, with the linear gradient providing the Fickian diffusion coefficient [36]. Conversely, a semi-logarithmic plot of $(1- (M(t) - M_0)/(M_\infty - M_0)$ versus time will be linear if the mass uptake is rate controlled by a first order process such as polymer relaxation (Equation 16). In the present experiments (see for example, Figure 4a

and 4b), a rapid initial period of Fickian diffusion is observed (ϕ_F) followed by an extended period of non-Fickian polymer relaxation (ϕ_R) and swelling as more carbon dioxide is absorbed into the membrane.

As also found by Wessling *et al.* [16] the proportion of the total sorption that occurs through Fickian processes is high at low pressures when the penetrant can be readily absorbed into the polymer structure. However, as the penetrant pressure increases, the polymer structure must swell as new voids are created to accommodate the penetrant molecules (Figure 5). Subsequently, Fickian diffusion decreases in importance and polymer relaxation processes become dominant. As these relaxation processes are much slower than Fickian diffusion, this leads to a rapid decline in the overall rate of sorption as penetrant concentration increases. Diffusion can only proceed as quickly as the polymer rearrangement will allow. This is contrary to the expected increase in rate predicted by the purely Fickian model described by Equation 9.

There is little evidence that the proportion of Fickian diffusion is affected by temperature. This might have been expected as the total penetrant solubility at a given gas fugacity is a strong function of temperature. However, instrument limitations meant that it was difficult to evaluate the rate of approach to equilibrium solubility at 77 ^{o}C and hence it was not possible to accurately report polymer relaxation data at this temperature.

The kinetics of the Fickian contribution to sorption occurs too rapidly to be accurately captured by these sorption experiments. However, the characteristic polymer relaxation time (τ_R) and the associated relaxation rate constant (K_R) can readily be quantified. As previously identified by Wessling *et al.* [16], this polymer relaxation time is not a function of penetrant pressure. There is however a temperature dependence, typical of Arrhenius kinetics (Table 4 and Figure 6). The activation energy associated with the relaxation rate constant is 16.7 kJmol^{-1}. The relaxation times are longer, but of a similar order of magnitude to that found by Wind *et al.* [14] for 1,4-cyclohexanedimethanol monoester samples of 40 - 60 μm (5.8 to 6.8 hours at 22 ^{o}C) and Wessling *et al.* [16] for a 6FDA based polymer sample of 60 μm (2.5 hours at 35 ^{o}C). The longer times probably reflect the different polymer structures, as well as both sorption and membrane preparation protocols. In particular, plasticization effects are known to be thickness dependent[37] and so the longer relaxation times may reflect differences in membrane

thickness. The selective layer in membranes used in industrial practice is much thinner and so may yield significantly different relaxation times.

Permeability

Figure 7 and Table 5 present data describing the variation of gas permeability with temperature for a number of permanent gases. Measurements were made over the temperature range 3°C – 112 °C, and at a constant pressure of 1000 kPa. The absolute magnitude of the permeability for the present membranes is within the range of literature reports. This permeability is a strong function of the membrane preparation and curing conditions, as well as the cooling rate after curing. In the present study, relatively mild membrane curing temperatures were used. Higher curing temperatures, such as those used by Tanaka *et al.* [2] and Lin and Chung [3], leads to greater compaction of the membrane structure and consequently a lower fractional free volume.

Since solubility generally decreases with increasing temperature, while diffusivity increases, the relative magnitudes of the two will dictate whether the overall permeability process is exothermic or endothermic. In the present case, nitrogen, and to a lesser extent oxygen permeability increases with temperature, consistent with the work of Lin & Chung [3]. Conversely, CO_2 permeability declines with temperature.

The permeability variation with fugacity displays the characteristic parabolic curve shape indicative of a plasticizing membrane material (Figure 8). At low fugacities, the influence of solubility dominates, with permeability declining as solubility declines. However, as the fugacity increases, the increase in gaseous diffusion occurring from enhanced free volume overwhelms the decrease in solubility coefficient and the permeability increases again. The turning point is often referred to as the plasticization pressure, or in this case, the plasticization fugacity.

It should be noted that the permeability recorded at pressures beyond the plasticization fugacity is not completely stable but increases slowly over a period of up to several hours due to the polymer relaxation processes described above. As permeabililty measurements were taken after only 30-55 minutes after each pressure change, the value recorded will underestimate the final pseudo-equilibrium value. This effect will be vanishingly small at low fugacities and high temperatures, but increase in importance at high fugacities and low temperatures.

Consistent with other workers, increased operating temperatures leads to elevated plasticization pressures [12, 13]. This is due to decreasing penetrant solubility at higher temperatures. Figure 9 shows that this turning point can be modeled using an Arrhenius approach with a logarithmic relationship between plasticization fugacity and 1/T.

Bos *et al.* [12] suggest that the concentration of CO_2 at the plasticization pressure is a constant for all polymers within a particular family, for example polycarbonates or polyimides. These workers suggest that generally polyimides require a CO_2 concentration of 36 ± 7 $cm^3_{(STP)}cm^{-3}_{polymer}$ to induce plasticization at 35 °C. Conversely, Wind *et al.* [15] indicated that the plasticization at 35 °C of 6FDA-DAM:DABA 2:1 copolymer did not occur at a particular CO_2 concentration. Rather, they found that plasticization at 35 °C occurred at a sorbed CO_2 partial molar volume of 29 ± 2 cm^3/mol in the polymer. According to these authors, reaching this critical partial molar volume allows for greater mobility in the normally well-packed Henry's Law region of the polymer structure.

For the present case, the concentration of CO_2 in 6FDA-TMPDA at the fugacity of plasticization has been plotted against temperature in Figure 10. It can be seen that plasticization is induced at lower concentrations when higher operating temperatures are utilized. Data indicates that when the operating temperature increases from 21°C to 77 °C, the CO_2 concentration necessary to induce plasticization drops from 91 $cm^3_{(STP)}cm^{-3}$ to 60 $cm^3_{(STP)}cm^{-3}$.

While the Langmuir concentration at the plasticization fugacity decreases with operating temperature, the Henry's Law component is essentially constant. This is consistent with the theory of Wind *et al.*[15], that it is this component that is most associated with plasticization effects. The Henry's Law concentration in this case, at 38 ± 2 $cm^3_{(STP)}cm^{-3}$, is within the range of values calculated from the data of Wind *et al.*[15], which range from 21 to 53 $cm^3_{(STP)}cm^{-3}$.

Chung *et al.* [38] suggest that the plasticization fugacity can be determined as the turning point in the curve of the overall heat of sorption H_s plotted as a function of fugacity. In the present case, a shallow turning point is observed in the heat of sorption at a fugacity of 1600 kPa (H_s = 13.9 $kJmol^{-1}$) and this value is within the range of plasticization fugacities presented in Figure 9. However, this approach assumes that the plasticization fugacity is independent of temperature and this does not appear to be the case for the present data set.

Diffusivity

The permeability data was analyzed in a more rigorous manner by assuming an exponential relationship for the diffusion coefficient with temperature (Equations 13 and 14). A least squares regression technique was used to generate the solid curves shown in Figure 4 using the sorption model data in Table 1. This generated the transport parameters summarized in Table 6.

The penetrant plasticizing ability (β) was found to fit an Arrhenius relationship with temperature (see Table 7). The recorded values are comparable to values reported in the literature (0.005 to 0.041 $cm^3cm^{-3}_{(STP)}$ for BPDA-DDBT polyimide [22]) which also found β to increase as temperature decreased.

The increasing value of F as temperature declines would suggest that while at high temperatures, diffusion is dominated by movement of Henry's law species, ($F \rightarrow 0$), at lower temperatures the movement of carbon dioxide molecules from the Langmuir sites is also becoming significant. The larger number and/or size of the Langmuir voids at these temperatures will lead to a greater number of pathways between such voids, thus allowing for more passage of molecules between these repositories of gas. Thus, while Langmuir species may not contribute to the swelling effects of plasticization, it is completely consistent that the movement of these species may contribute to the overall diffusion coefficient at lower temperatures.

As discussed above, the rate of increase in permeability at low temperatures may be underestimated in this work as a result of the long time scales of polymer relaxation. This will lead to a slight underprediction of the values of β and/or F at these lower temperatures. Consequently the activation energies recorded in Table 7 for these parameters are also likely to be a slight underestimate of the true value of this temperature sensitivity.

An Arrhenius relationship was also observed for the predicted diffusion coefficient at zero penetrant concentration D(0), as presented in Figure 11. The magnitude of diffusivities at zero penetrant concentration, are in good agreement with Okamoto *et al.*[13], who observed D(0) values of 3.4×10^{-8} to 9×10^{-8} cm^2s^{-1} over the temperature range 35 – 80 °C for a similar polyimide.

Figure 12 plots the simulated diffusion coefficient determined from Equation 13 and using these values of β, F and $D(0)$ as a function of both temperature and CO_2 fugacity. This shows that while the diffusion coefficient at zero penetrant concentration D(0) increases with temperature, this trend is rapidly overwhelmed by the much greater swelling due to plasticization at low temperatures, so that the diffusivity at higher fugacities decreases significantly with increasing temperature.

Conclusions

The polymer that is the focus of this study, 6FDA-TMPDA is a rigid glassy polyimide with a high glass transition temperature. Subsequently, plasticization has little effect on the total solubility of carbon dioxide across the range of temperatures studied, with a high proportion of the total dissolved penetrant present in large Langmuir voids. Conversely, the effect upon diffusivity is significant. As the concentration of dissolved carbon dioxide increases, the polymer swells through a process of polymer relaxation, causing an increase in the diffusion coefficient. Through kinetic sorption experiments, it was found that the proportion of total penetrant dissolution changes from being almost entirely Fickian at low penetrant pressures, to almost entirely through polymer relaxation at high pressures. However, this proportionality is relatively unaffected by temperature.

Based on permeation experiments, the diffusion coefficient can readily be modeled as an exponential function of penetrant concentration, and an Arrhenius function of temperature. This increasing diffusivity causes the permeability versus penetrant fugacity to have a characteristic parabolic shape. The turning point of this curve, the plasticization fugacity, also forms an Arrhenius relationship with temperature. Plasticization appears to occur at a constant Henry's law concentration of carbon dioxide across the full temperature range. The use of a more rigorous model shows that permeation through the membrane is dominated by diffusion through the Henry law region at high temperature, but as the number and/or size of the Langmuir voids increase at low temperatures, these species also contribute to diffusion processes.

Nomenclature

A	Constant in Equation 8 (cm^2s^{-1})
B	Constant in Equation 8
b	Langmuir hole affinity constant (atm^{-1})
C	Penentrant concentration in the polymer ($cm^3_{STP}cm^{-3}_{polym}$)
C_g	Isothermal glass transition concentration ($cm^3_{STP}cm^{-3}_{polym}$)
C'_H	Langmuir capacity constant ($cm^3_{STP}cm^{-3}_{polym}$)
$C'_H(0)$	Langmuir capacity constant at zero penetrant concentration ($cm^3_{STP}cm^{-3}_{polym}$)
C*	Effective penetrant concentration ($cm^3_{STP}cm^{-3}_{polym}$)
D_{eff}	Effective Fickian diffusion coefficient (cm^2s^{-1})
D	Fickian diffusion coefficient (cm^2s^{-1})
D(0)	Diffusion coefficient at zero penetrant concentration (cm^2s^{-1})
D_T	Thermodynamic diffusion coefficient (cm^2s^{-1})
E_A	Activation Energy ($kJ\ mol^{-1}$)
E_D	Activation Energy for diffusion ($kJmol^{-1}$)
E_P	Activation Energy for permeation ($kJmol^{-1}$)
F	Fraction of Langmuir species that are mobile
f	Fugacity (atm)
H_S	Heat of Sorption ($kJ\ mol^{-1}$)
J_s	Steady State Flux ($cm^3_{STP}cm^2s^{-1}$)
K	$C'_H.b/K_D.$
K_D	Henry's Law Constant ($cm^3_{STP}cm^{-3}_{polym}atm^{-1}$)
M	sorbed mass uptake (g)
P	Permeability (cm^3_{STP} cm cm^{-2} s^{-1} atm^{-1})
R	Universal gas constant ($J\ mol^{-1}K^{-1}$)
S	Solubility ($cm^3_{STP}cm^{-3}_{polym}atm^{-1}$)

Greek Letters

β	Plasticizing ability of penetrant ($cm^3_{polym}cm^{-3}_{(STP)}$)
δ	Membrane thickness (cm)
ϕ_F	Fickian contribution to the fractional sorbed mass uptake
ϕ_R	Relaxational contribution to the fractional sorbed mass uptake

σ	Parameter characterizing the concentration dependence of the Henry's Law dissolution ($cm^3_{polym}cm^{-3}_{STP}$)
τ_R	Relaxation time (hr)
υ_f	Polymer fractional free volume

Subscripts

D	dissolved or Henry's Law component
H	adsorbed or Langmuir component
o	indicates a pre-exponential factor in an Arrhenius relationship
0	value at time = 0
1	feed conditions
2	permeate conditions
∞	value at infinite time (Equation 15)

References:

1. Y. Kamiya, K. Mizoguchi, T. Hirose, and Y. Naito, Sorption and dilation in poly(ethyl methacrylate)-carbon dioxide system. Journal of Polymer Science, Part B: Polymer Physics, 27(4) (1989) 879-92.
2. K. Tanaka, M. Okano, H. Toshino, H. Kita, and K. Okamoto, Effect of methyl substituents on permeability and permselectivity of gases in polyimides prepared from methyl-substituted phenylenediamines. J. Polymer Sci., Part B: Polymer Physics, 30(8) (1992) 907-14.
3. W.-H. Lin and T.-S. Chung, Gas permeability, diffusivity, solubility, and aging characteristics of 6FDA-durene polyimide membranes. J. Membrane Sci, 186(2) (2001) 183-193.
4. W.-H. Lin, R.H. Vora and T.-S. Chung, Gas transport properties of 6FDA-durene/1,4-phenylenediamine (pPDA) copolyimides. J. Polymer Sci. Part B: Polymer Physics, 38(21) (2000) 2703-2713.
5. T.-S. Chung, W.-H. Lin and R.H. Vora, Gas transport properties of 6FDA-durenediamine/1,3-phenylenediamine (mPDA) copolyimides. J. Applied Polymer Sci. 81(14) (2001) 3552-3564.
6. K. Nagai, N. Booker, A. Mau, J. Hodgkin, S. Kentish, G. Stevens, and A. Geertsema, Gas Permeation Properties of Polyimide/Epoxy Composite Materials. Polymeric Materials: Science & Engineering, 85(1) (2001) 91.
7. Y. Liu, M.L. Chung, T.-S. Chung and R. Wang, Effects of amidation on gas permeation properties of polyimide membranes. J. Membrane Sci. 214(1) (2003) 83-92.
8. A. Bos, High pressure CO_2/CH_4 separation with glassy polymer membranes - Aspects of CO_2-induced plasticization, PhD Dissertation, (1996) Department of Chemical Technology, University of Twente.

9. A. Bos, I.G.M. Pont, M. Wessling and H. Strathmann, Suppression of CO2-plasticization by semi-interpenetrating polymer network formation. J. Polymer Sci. Part B: Polymer Physics, 36(9) (1998) 1547-1556.

10. A. Bos, I. Punt, H. Strathmann and M. Wessling, Suppression of gas separation membrane plasticization by homogeneous polymer blending. AIChE Journal, 47(5) (2001) 1088-1093.

11. A. Bos, I.G.M. Punt, M. Wessling and H. Strathmann, Plasticization-resistant glassy polyimide membranes for CO_2/CH_4 separations. Sep.& Purificat. Technol. 14(1-3) (1998) 27-39.

12. A. Bos, I.G.M. Punt, M. Wessling, and H. Strathmann, CO2-induced plasticization phenomena in glassy polymers. J. Membrane Sci, 155(1) (1999) 67-78.

13. K.-I. Okamoto, K. Tanaka, T. Shigematsu, H. Kita, A. Nakamura and Y. Kusuki, Sorption and transport of carbon dioxide in a polyimide from 3,3',4,4'-biphenyltetracarboxylic dianhydride and dimethyl-3,7-diaminodibenzothiophene-5,5'-dioxide. Polymer, 31(4) (1990) 673-678.

14. J.D. Wind, S.M. Sirard, D.R. Paul, P.F. Green, K.P. Johnston and W.J. Koros, Relaxation dynamics of CO2 diffusion, sorption, and polymer swelling for plasticized polyimide membranes. Macromolecules, 36(17) (2003) 6442-6448.

15. J.D. Wind, S.M. Sirard, D.R. Paul, P.F. Green, K.P. Johnston, and W.J. Koros, Carbon dioxide-induced plasticization of polyimide membranes: pseudo-equilibrium relationships of diffusion, sorption, and swelling. Macromolecules, 36(17) (2003) 6433-6441.

16. M. Wessling, I. Huisman, T.V.D. Boomgaard, and C.A. Smolders, Dilation Kinetics of Glassy Aromatic Polyimides Induced by Carbon Dioxide Sorption. J. of Polymer Sci. Part B: Polymer Physics, 33 (1995) 1371-1364.

17. J. H. Petropoulos, Mechanisms and Theories for Sorption and Diffusion of Gases in Polymers in D.R. Paul and Y.P. Yampolskii (Eds.) Polymeric Gas Separation Membranes Boca Raton: CRC Press (1994) pp. 17 – 81.

18. L.M. Costello and W.J. Koros, Thermally stable polyimide isomers for membrane-based gas separations at elevated temperatures. J. Polymer Sci. Part B: Polymer Physics, 33(1) (1995) 135-46.

19. S. Kanehashi and K. Nagai, Analysis of dual-mode model parameters for gas sorption in glassy polymers. J. Membrane Sci. 253 (2005) 117-138.

20. J.S. Chiou, Y. Maeda and D.R. Paul, Gas and vapor sorption in polymers just below T_g. J. Appl. Polymer Sci. 30(10) (1985) 4019-29.

21. Y. Kamiya, T. Hirose, K. Mizoguchi and Y. Naito, Gravimetric study of high-pressure sorption of gases in polymers. J. Polymer Sci. Part B: Polymer Physics, 24(7) (1986) 1525-39.

22. R.J. Pace and A. Datyner, The temperature dependence of the Langmuir capacity factor in glassy polymers. J. Polymer Sci., Polymer Physics, 19(10) (1981) 1657-8.

23. J.H. Petropoulos, Quantitative analysis of gaseous diffusion in glassy polymers. J. Polymer Sci. Polymer Physics 8(10) (1970) 1797-801.

24. N. Platé, Y. Yampol'skii, Relationship between Structure and Transport Properties for High Free Volume Polymeric Materials in D.R. Paul and Y.P. Yampolskii, (Eds.) Polymeric gas separation membranes. Boca Raton: CRC Press (1994) pp. .

25. H. Fujita, Fortschr. Hochpolym. Forsch. 3 (1961) 1.

26. J. Crank and G.S. Park, An evaluation of the diffusion coefficient for chloroform in polystyrene from simple absorption experiements. Trans. Faraday Soc. 45 (1948) 240-249.

27. R.M. Barrer, Some Properties of Diffusion Coefficients in Polymers. J. Phys. Chem. 61(February) (1957) 178-189.

28. D.R. Paul. and W.J. Koros, Effect of partially immobilizing sorption on permeability and the diffusion time lag. J. Polymer Sci. Polymer Physics 14(4) (1976) 675-85.

29. S.A. Stern and V. Saxena, Concentration-Dependent Transport of Gases and Vapors in Glassy Polymers. J. Membrane Sci. 7 (1980) 47-59.

30. A.R. Berens and H.B. Hopfenberg, Diffusion and Relaxation in glassy polymer powders: 2. Separation of diffusion and relaxation parameters. Polymer, 19(May) (1978) 489-496.

31. C.E. Powell, X.J. Duthie, S.E. Kentish, G.G. Qiao, and G.W. Stevens, Reversible Diamine Cross-Linking of Polyimide Membranes. J Membrane Sci, Submitted 2006.

32. Y. Liu, R. Wang and T.-S. Chung, Chemical cross-linking modification of polyimide membranes for gas separation. J. Membrane Sci. 189(2) (2001) 231-239.

33. S.L. Liu, R. Wang, T.S. Chung, M.L. Chung, Y. Liu and R.H. Vora, Effect of diamine composition on the gas transport properties in 6FDA-durene/3,3'-diaminodiphenyl sulfone copolyimides. J. Membrane Sci. 202(1-2) (2002) 165-176.

34. S.I. Sandler, Chemical, Biochemical and Engineering Thermodynamics, 4th Edition,. John Wiley & Sons (2006) pp. 250-252

35. L. Shao, T.-S. Chung, S.H. Goh, and K.P. Pramoda, The effects of 1,3-cyclohexanebis(methylamine) modification on gas transport and plasticization resistance of polyimide membranes. J. Membrane Sci, 267(1-2) (2005) 78-89.

36. C.E. Rogers, Solubility & Diffusivity, in D. Fox, M.M. Labes and A. Weissberger, (Eds.) Physics and chemistry of the organic solid state, , John Wiley & Sons New York (1965) p. 975.

37. M. Wessling, M. Lidon Lopez, H. Strathmann, Accelerated plasticization of thin-film composite membranes used in gas separation. Sep. & Purificat. Technol., 24(1-2) (2001) 223-233.

38. T.-S. Chung, C. Cao and R. Wang, Pressure and Temperature Dependence of the Gas Transport Properties of Dense Poly[2,6-toluene-2,2-bis(3,4-dicarboxylphenyl)hexafluoropropane diimide] Membranes J. Polymer Sci. Part B: Polymer Physics. 42 (2004) 354-364

List of Table Captions

Table 1 Permeability Isotherm Measurement Protocol

Table 2 Dual Mode Sorption Parameters for 6FDA-TMPDA at 0 – 40 Bar

Table 3 Temperature Dependence of Dual Mode Sorption parameters of CO_2 in 6FDA-TMPDA

Table 4 – Kinetic parameters for relaxation of 6FDA-TMPDA upon exposure to carbon dioxide based on sorption mass uptake.

Table 5. Thermodynamic permeation data determined for 6FDA-TMPDA at 1000kPa, 35 ^{o}C

Table 6 Transport Parameters for CO_2 transport in 6FDA-TMPDA at various operating temperatures based on Equation 14. Error estimates are based on standard error estimates generated during the non-linear fit (95% confidence interval based on a t-distribution).

Table 7 Activation energy estimates for concentration dependant diffusion parameters

Table 1

Penetrant	Absolute Feed Pressure (kPa)	Exposure time (minutes)
System Evacuation	0	720 (minimum)
Nitrogen	1000	30
Oxygen	1000	30
Methane	1000	30
Carbon Dioxide	330	30
	660	30
	1000	30
	1500	30
	2000	55
	2500	55
	3000	55

Table 2

	Fugacity Based Model				Pressure Based Model	
Temperature (°C)	21	35	50	77	35	Shao *et al.* [35] 35°C
K_D ($cm^3_{(STP)}cm^{-3}atm$)	4.6	3.2	2.4	1.6	2.3	2.66
C'_H ($cm^3_{(STP)}cm^{-3}$)	62.9	58.8	47.7	34.1	72.2	52.43
b (atm^{-1})	0.94	0.55	0.33	0.29	0.39	0.741

Table 3

	K_D		C'_H		b	
	K_{Do} ($cm^3cm^{-3}atm^{-1}$)	H_{SD} (kJ/mol)	C'_{Ho} (cm^3cm^{-3})	H_{SH} (kJ/mol)	b_o atm^{-1}	E_A (kJ/mol)
Fugacity Basis Current Study	0.0064	-16.0	1.26	-9.7	0.00051	-18.0
Pressure Basis Current Study	0.0105	-13.9	1.33	-10.1	0.0011	-15.1
Pressure basis Okamoto [13] (BTDA polymer)	-	-11.9	-	-	-	-20.0

Table 4

Temperature (°C)	Relaxation Rate Constant (K_R) ($cm^2\ s^{-1}$)	Relaxation Time (τ_R) (hours)
21	2.09×10^{-10}	21.8
35	2.90×10^{-10}	15.7
50	3.85×10^{-10}	11.8

Table 5

	Permeability (Barrer)			P_o (Barrer)			E_p (kJ/mol)		
	CO_2	N_2	O_2	CO_2	N_2	O_2	CO_2	N_2	O_2
Current Study	577	47	157	165	183	175	-3.3	3.5	0.32
Tanaka *et al.* [2]	440	-	-	-	-	-	-1.3	-	-
Lin & Chung [3]	440	35.6	122	-	-	-	0.2	4.45	2.4
Shao *et al.*[35]	612	55.4	186	-	-	-	-	-	-

Table 6

Temperature (°C)	D(0) (x 10^{8} $cm^{2}sec^{-1}$)	β ($cm^{3}cm^{-3}_{[STP]}$)	F
21	0.36 ± 0.35	0.027 ± 0.004	0.52 ± 0.18
35	0.51 ± 0.35	0.024 ± 0.004	0.57 ± 0.18
50	1.6 ± 0.35	0.015 ± 0.004	0.26 ± 0.18
77	32 ± 0.35	0.006 ± 0.004	0.09 ± 0.18

Table 7

Process	Activation Energy ($kJmol^{-1}$)
D (0)	35.4
B	-24.9
F	-28.4
Plasticization Fugacity	14.8
Relaxation rate constant (K_R)	16.7

List of Figure Captions

Figure 1 Poly(4,4'-hexafluoroisopropylidene diphthalic anhydride - 2,3,5,6-tetramethyl-1,4-phenylenediamine) (6FDA-TMPDA) polyimide.

Figure 2 Diagram of the constant volume, variable pressure permeability apparatus

Figure 3 CO_2 sorption isotherm for 6FDA-TMPDA. Symbols represent experimental data while solid lines represent the dual mode sorption model given by Equation 5 with parameters as given in Table 2

Figure 4 Approach of a membrane sample to the equilibrium solubility. The membrane sample is at 35C and the pressure has been increased from 2.6 to 5.2 Bar carbon dioxide (a) Expressed as a plot of fractional mass uptake $(M(t) - M_0)/(M_\infty - M_0)$ versus time$^{1/2}$ (b) Expressed on the basis of first order kinetics (see Equations 14 and 15)

Figure 5 Proportion of the sorption mass uptake during kinetic sorption experiments than can be related to Fickian diffusion (ϕ_F) rather than polymer relaxation (ϕ_R) as a function of CO_2 fugacity.

Figure 6 Arrhenius plot of the polymer relaxation rate constant

Figure 7 Permanent gas permeability in 6FDA-TMPDA recorded at 1000 kPa

Figure 8 CO_2 permeability of 6FDA-TMPDA as a function of fugacity at various temperatures. Symbols represent experimental data while solid curves are based on Equation 13, with parameters from Table 6.

Figure 9 Plasticization Fugacity versus reciprocal temperature for 6FDA-TMPDA

Figure 10 CO_2 concentration at the plasticization fugacity.

Figure 11 Arrhenius plot of the diffusion coefficient at zero penetrant concentration D(0) as predicted from Equation 14.

Figure 12 Plot of the Fickian diffusion coefficient as a function of temperature and CO_2 fugacity. Values were calculated using Equation 13 and the parameters provided in Table 6.

Figure 1

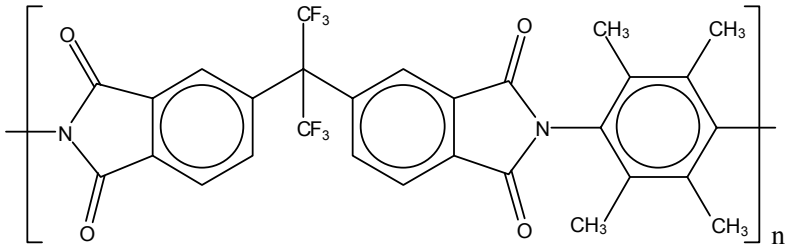

Figure 2

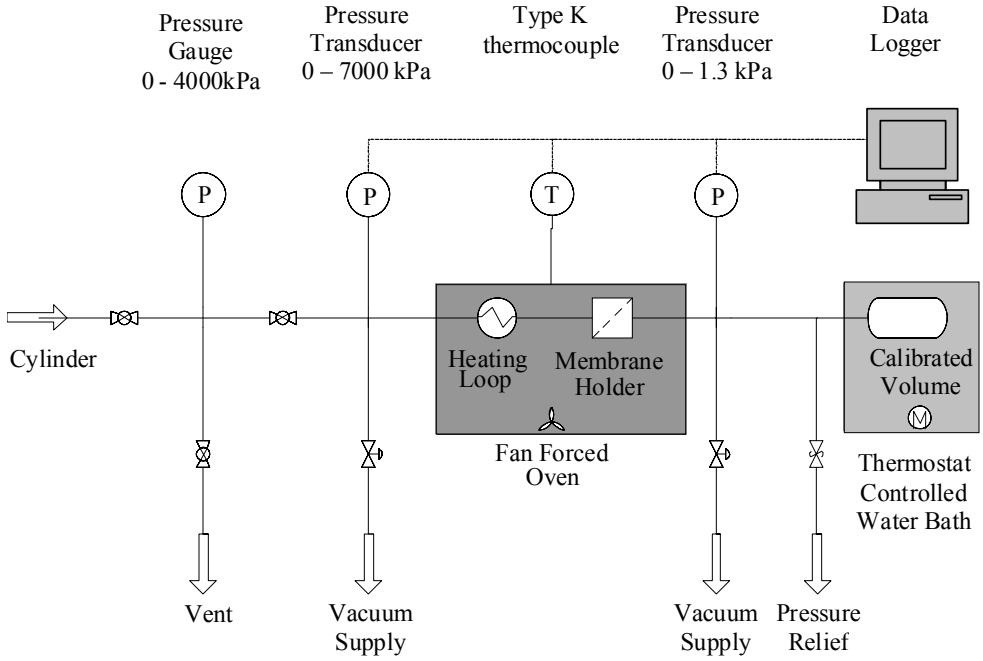
Pressure Gauge 0 - 4000kPa
Pressure Transducer 0 – 7000 kPa
Type K thermocouple
Pressure Transducer 0 – 1.3 kPa
Data Logger
P
P
T
P
Cylinder
Heating Loop
Membrane Holder
Fan Forced Oven
Calibrated Volume
M
Thermostat Controlled Water Bath
Vent
Vacuum Supply
Vacuum Supply
Pressure Relief

Figure 3

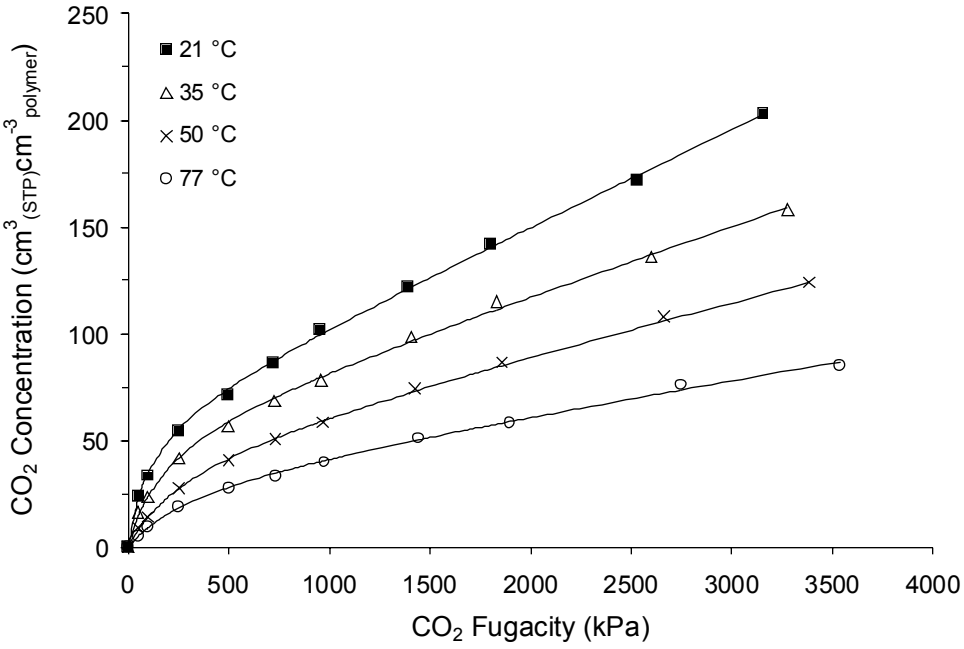
250
200
150
100
50
0
21 °C
35 °C
50 °C
77 °C
0
500
1000
1500
2000
2500
3000
3500
4000
CO2 Concentration (cm3(STP)cm-3polymer)
CO2 Fugacity (kPa)

Figure 4

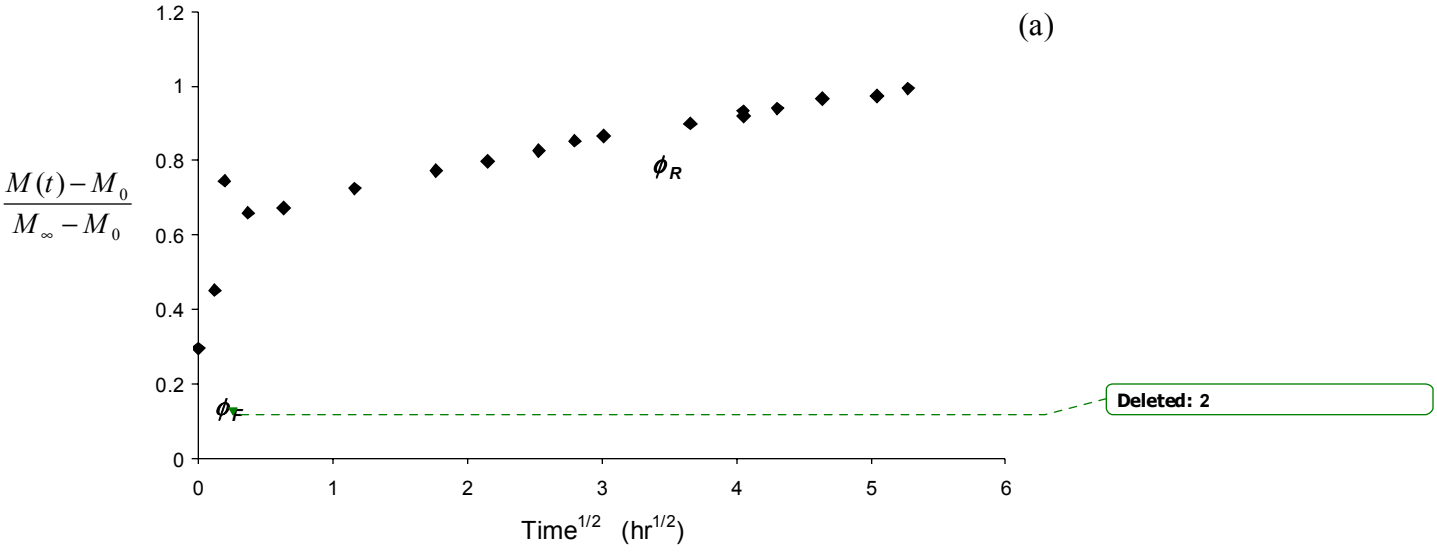

Deleted: 2

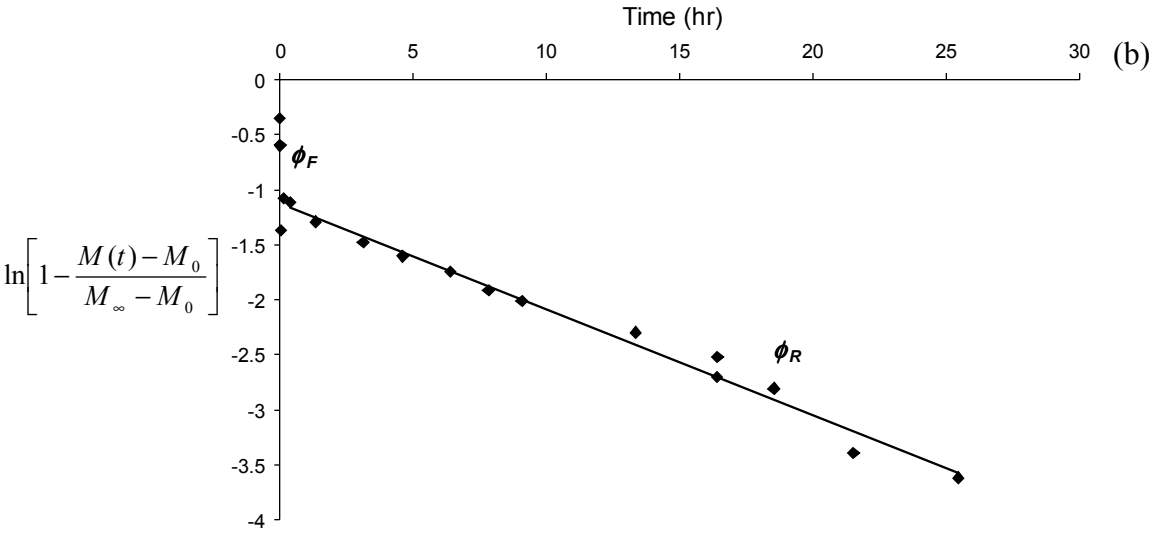

Figure 5

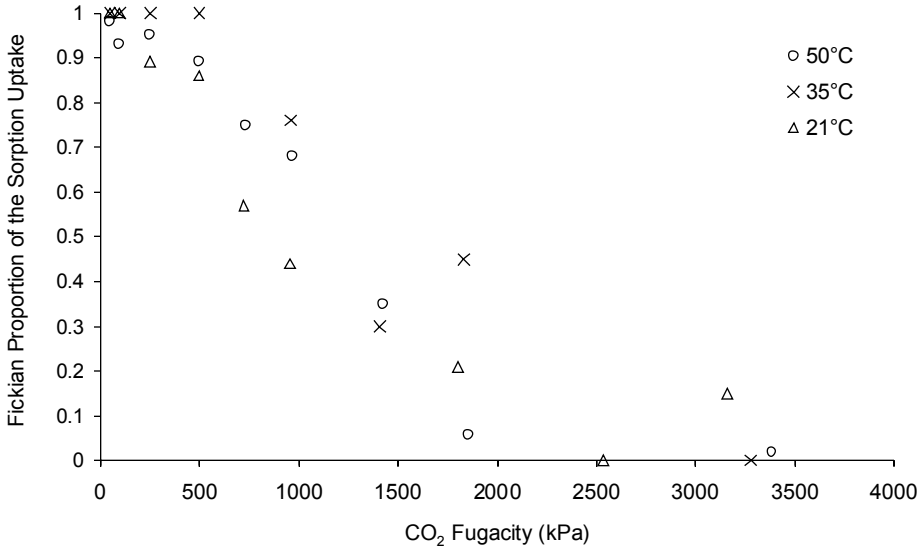
Fickian Proportion of the Sorption Uptake
1
0.9
0.8
0.7
0.6
0.5
0.4
0.3
0.2
0.1
0
0
500
1000
1500
2000
2500
3000
3500
4000
CO2 Fugacity (kPa)
50°C
35°C
21°C

Figure 6

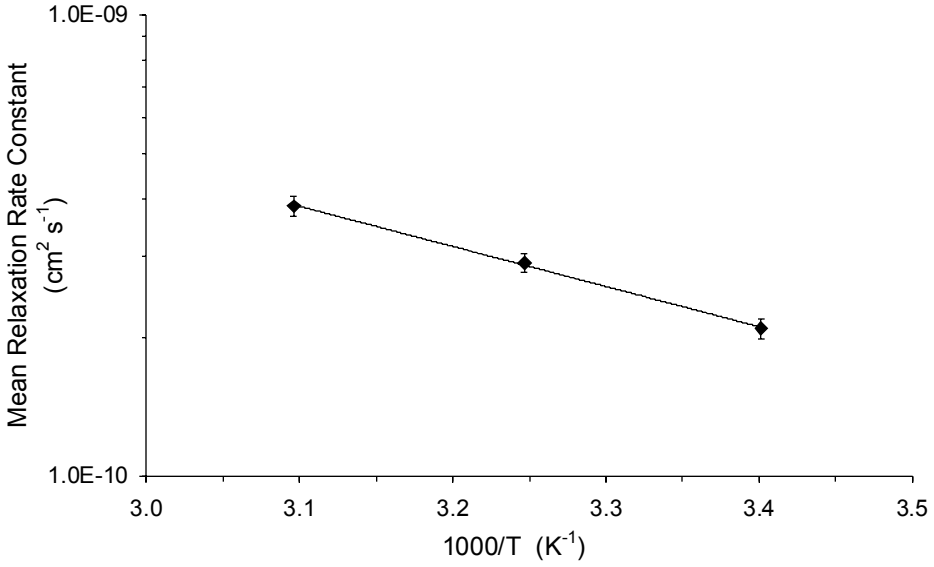
1.0E-09
1.0E-10
Mean Relaxation Rate Constant
(cm2 s-1)
3.0
3.1
3.2
3.3
3.4
3.5
1000/T (K-1)

Figure 7

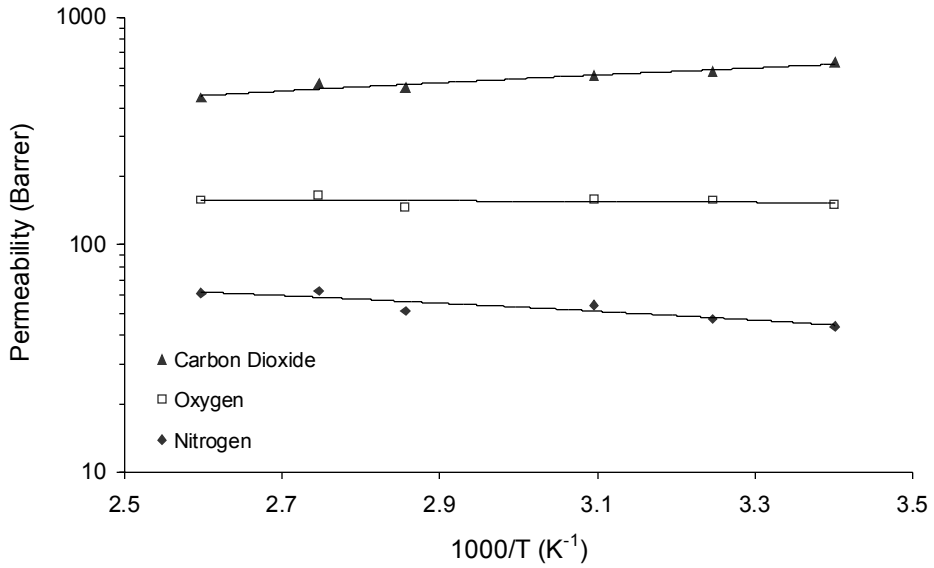
1000
100
10
Permeability (Barrer)
Carbon Dioxide
Oxygen
Nitrogen
2.5
2.7
2.9
3.1
3.3
3.5
1000/T (K-1)

Figure 8

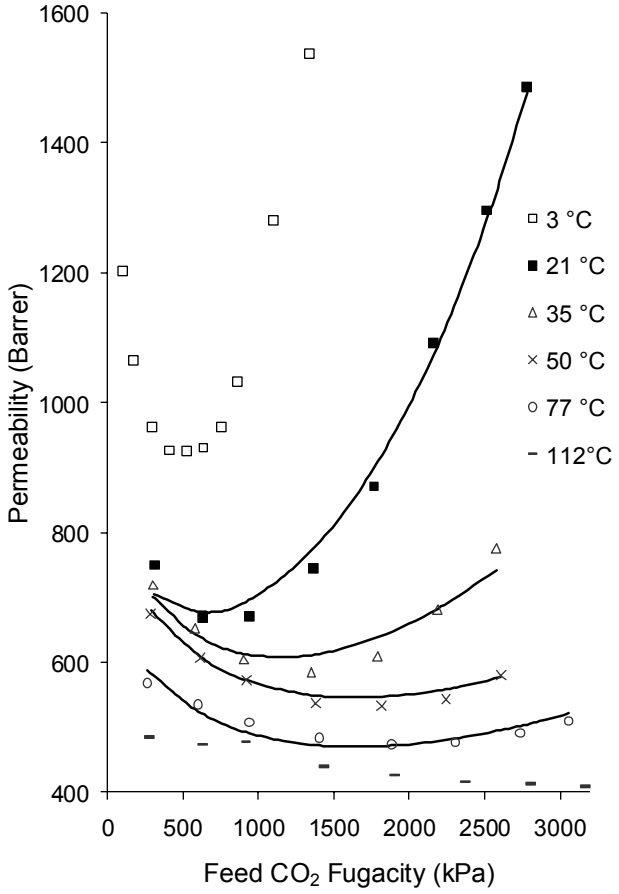
1600
1400
1200
1000
800
600
400
Permeability (Barrer)
0
500
1000
1500
2000
2500
3000
Feed CO_2 Fugacity (kPa)
3 °C
21 °C
35 °C
50 °C
77 °C
112°C

Figure 9

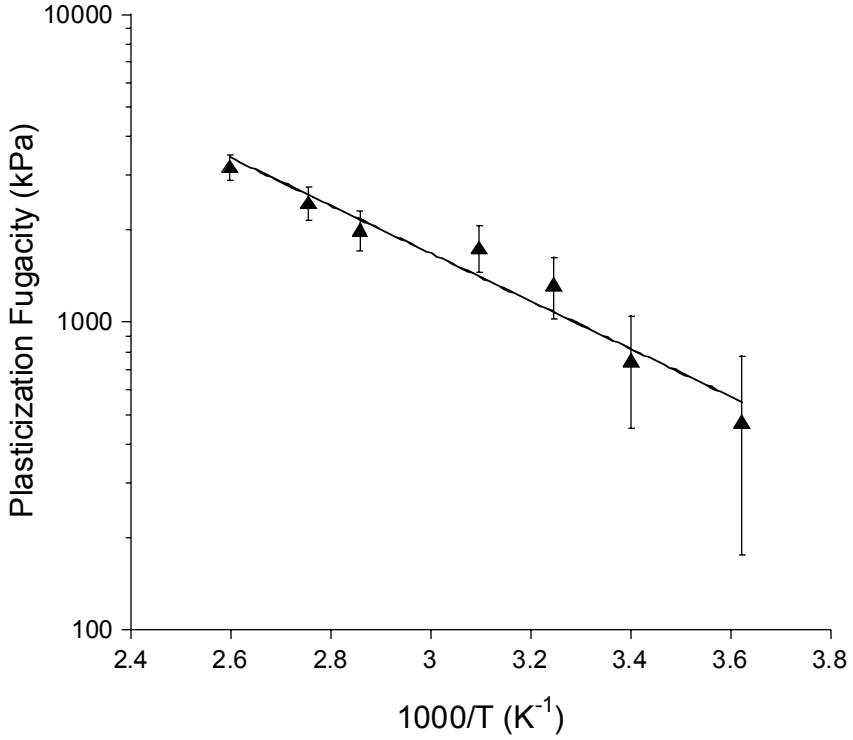
10000
1000
100
Plasticization Fugacity (kPa)
2.4
2.6
2.8
3
3.2
3.4
3.6
3.8
1000/T (K-1)

Figure 10

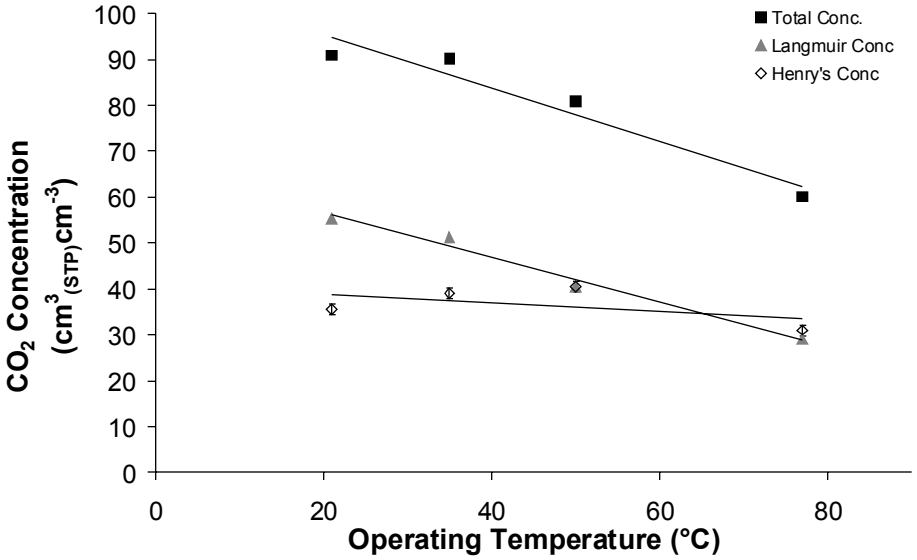
Total Conc.
Langmuir Conc
Henry's Conc
CO_2 Concentration ($cm^3_{(STP)}cm^{-3}$)
Operating Temperature (°C)
0
10
20
30
40
50
60
70
80
90
100
0
20
40
60
80

Figure 11

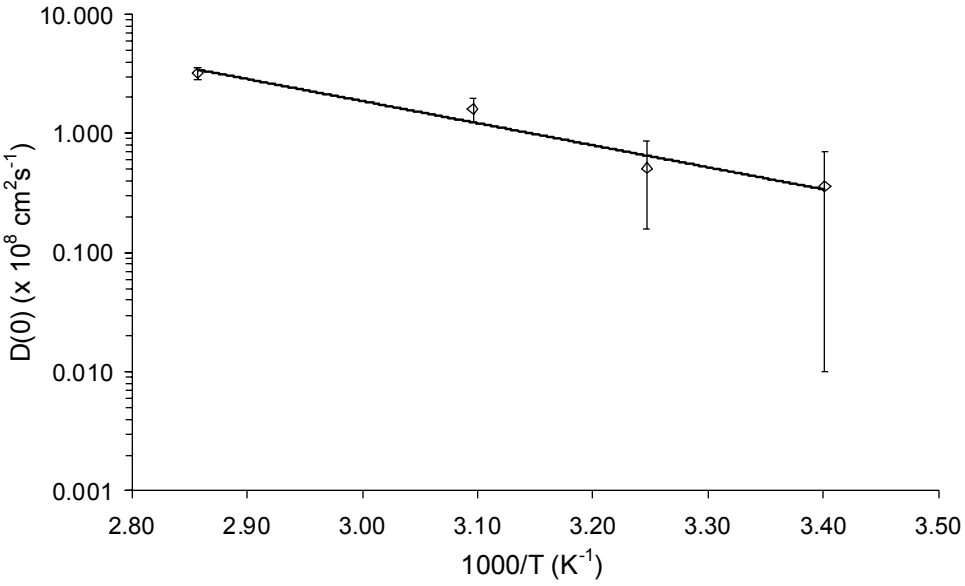
10.000
1.000
0.100
0.010
0.001
D(0) (x 10^8 cm^2s^-1)
2.80
2.90
3.00
3.10
3.20
3.30
3.40
3.50
1000/T (K^-1)

Figure 12

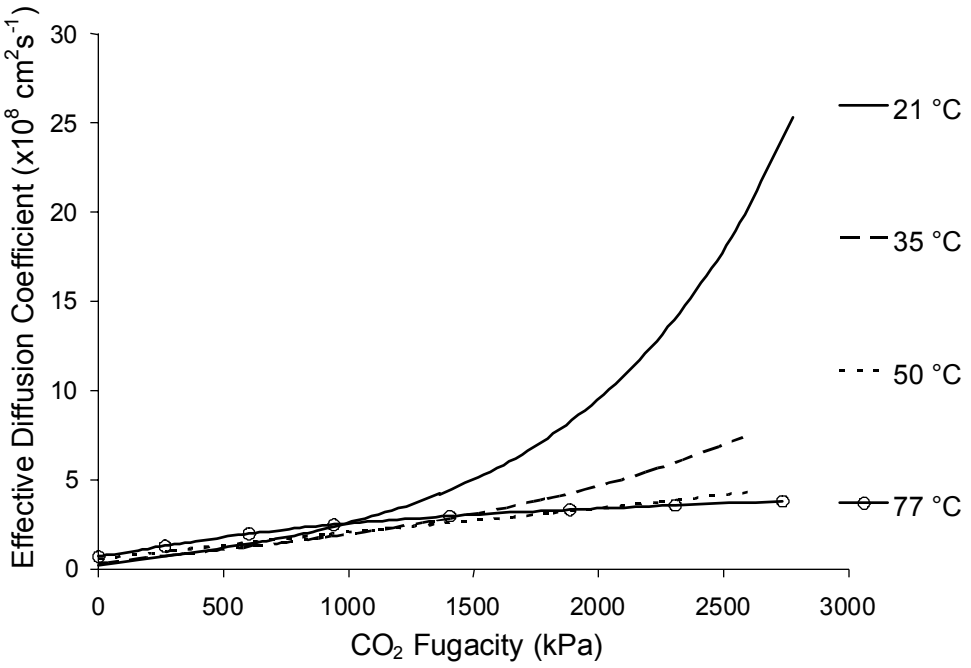
Effective Diffusion Coefficient (x10^8 cm^2s^-1)
30
25
20
15
10
5
0
0
500
1000
1500
2000
2500
3000
CO2 Fugacity (kPa)
21 °C
35 °C
50 °C
77 °C